European Journal of Mechanics A/Solids 28 (2009) 516–525

Contents lists available at ScienceDirect

European Journal of Mechanics A/Solids

www.elsevier.com/locate/ejmsol

Delay effects in shimmy dynamics of wheels with stretched string-like tyres

Dénes Takács [a,1,*], Gábor Orosz [b,2], Gábor Stépán [a,1]

[a] Department of Applied Mechanics, Budapest University of Technology and Economics, PO Box 91, Budapest H-1521, Hungary
[b] Department of Mechanical Engineering, University of California, Santa Barbara, CA 93106, USA

ARTICLE INFO

Article history:
Received 30 August 2007
Accepted 26 November 2008
Available online 7 December 2008

Keywords:
Shimmy
Delay
Relaxation length
Travelling wave solution
Hopf bifurcation

ABSTRACT

The dynamics of wheel shimmy is studied when the self-excited vibrations are related to the elasticity of the tyre. The tyre is described by a classical stretched string model, so the tyre-ground contact patch is approximated by a contact line. The lateral deformation of this line is given via a nonholonomic constraint, namely, the contact points stick to the ground, i.e., they have zero velocities. The mathematical form of this constraint is a partial differential equation (PDE) with boundary conditions provided by the relaxation of deformation outside the contact region. This PDE is coupled to an integro-differential equation (IDE), which governs the lateral motion of the wheel. Although the conventional stationary creep force idea is not used here, the coupled PDE-IDE system can still be handled analytically. It can be rewritten as a delay differential equation (DDE) by assuming travelling wave solutions for the deformation of the contact line. This DDE expresses the intrinsic *memory effect of the elastic tyre*. The linear stability charts and the corresponding numerical simulations of the nonlinear system reveal periodic and quasi-periodic self-excited oscillations that are also confirmed by simple laboratory experiments. The observed quasi-periodic vibrations cannot be explained in single degree-of-freedom wheel models subject to a creep force.

1. Introduction

The lateral vibration of towed wheels, called shimmy, may appear on airplane landing gears, motorcycle wheels, caravans, rear wheels of semi-trailers and articulated buses, and it usually presents a safety hazard. The terminology 'shimmy' appeared in the 1920's when it was the name of a popular dance. The shimmy of towed wheels may be caused either by the elasticities of the towing bar suspension and the attached vehicle structure, or by the elasticity of the tyre on the wheel, or by a combination of the two cases. There are two important reasons why the shimmy phenomenon has not been fully explored yet. One part of the problem is that the vehicle itself is a complex dynamical system serving several low-frequency vibration modes which may all be important components of the dynamical behaviour at different running speeds and conditions. This part of the problem is mainly resolved by the development of multibody dynamics and commercial computer codes (Schiehlen, 2006). The other part of the problem is originated in the wheel-ground contact. Advanced finite element calculations need long computation times even in stationary cases; see Kalker (1991) for railway wheels and Böhm (1989), Chang et al. (2004) for tyres. Even nowadays, the dynamic contact problems usually require special codes, large computational power, and still, there are no analytical results available to check these calculations.

One of the first scientific reports on shimmy was presented by von Schlippe and Dietrich (1941), where they analysed a simple low degree-of-freedom (DoF) model. In this so-called *stretched string model* the tyre-ground contact was considered as a contact line that becomes deformed due to the lateral displacement of the wheel (see the curve between the points L and R in Fig. 1), while the longitudinal deformation was neglected. Furthermore, it was considered that each contact point P sticks to the ground. Note that the tyre becomes deformed not only along the contact line but also in front of the leading point L and behind the rear point R as represented by the deformed central line of the tyre in Fig. 1. It was assumed that outside the contact patch the deformation decays exponentially, which was also confirmed by measurements. Because the resulting equations were too complicated to be analysed with the available mathematical tools at that time, they introduced a severe simplification, namely, the contact line was straight between the points L and R. This way, the resultant lateral force and torque induced by the elastic tyre deformation were calculated, leading to a delay differential equation (DDE) with a *discrete delay*. Using this equation the linear stability of the stationary rolling motion was analysed (with some further simplifications since the mathematical theory of DDEs was not available

* Corresponding author.
E-mail addresses: takacs@mm.bme.hu (D. Takács), gabor@engineering.ucsb.edu (G. Orosz), stepan@mm.bme.hu (G. Stépán).
[1] Research Group on Dynamics of Vehicles and Machines, Hungarian Academy of Sciences, PO Box 91, Budapest H-1521, Hungary.
[2] Mathematics Research Institute, School of Engineering, Computer Science and Mathematics, University of Exeter, EX4 4QF, United Kingdom.

0997-7538/$ – see front matter
doi:10.1016/j.euromechsol.2008.11.007

at that time). The discrete delay was equal to the time period of a tyre point while in contact with the ground between L and R. Since then, several versions of the stretched string model have been developed and analysed. For example, in Segel (1966) frequency response functions were calculated for the stretched string model without any restriction to the shape of the contact line. This so-called *exact stretched string model* has become a basic reference for later studies. This approach results in a DDE with a *distributed delay* as explained in details in Section 3.

A different approach was taken by Pacejka (1966) who introduced different straight and curved contact line approximations by using stationary shape functions for the lateral tyre deformation calculated at constant drift angles. The resultant lateral creep force and torque are calculated from these 'quasi-stationary' deformations by the semi-empirical 'Magic Formula' (Pacejka, 2002). This way, the delay effects are completely eliminated. In the resulting simplified models only the caster angle and the lateral deformation of the leading point L were used as state variables, leading to an ordinary differential equation (ODE) that made it very popular and easy-to-analyse. In the middle range of the towing speeds, the quasi-stationary deformation idea gives reasonable agreement with experiments. Several research reports prove the success of this approach in engineering (see Troger and Zeman, 1984, on tractor-semi-trailers systems, Sharp et al., 2004, on motorcycles or Fratila and Darling, 1996 on caravans). Nonlinearities were also introduced and their importance were emphasised by the existence of unstable periodic motions in Pacejka (1966). The model was also generalised by considering the effect of the width of the contact area, that of sliding at the rear part of the contact patch, and that of the gyroscopic effects appearing when the wheel is allowed to be tilted from its vertical plane. Pacejka's wisdom about tyres has accumulated in his book (Pacejka, 2002) that also includes a separate chapter for shimmy with an extensive reference list.

Considering the exact stretched string model with simplified boundary conditions, Stépán (1998) has introduced nonlinearities into the system. He also investigated the linear stability with mathematical rigour leading to the possibilities of quasi-periodic oscillations, which recently has been confirmed experimentally in Takács (2005), Takács and Stépán (2007).

The elasticity of the tyre was also considered in a *point contact model* by Moreland (1954). The contact line was shrunk into a point where the force, induced by the elastic tyre, acts. A relaxation time was also introduced for the force to model its 'delayed action' and a torque coefficient was defined to relate the force and the torque. It was proven by Collins (1971) that the point contact model is equivalent to the stretched string model when the latter is restricted to the case of straight contact line. However, in the point contact model the relaxation time and a torque coefficient has to be estimated or measured, while the stretched string model provides the corresponding constants via its geometry.

If there is elasticity in the suspension system, even a point contact model with rigid tyre can exhibit shimmy and complicated nonlinear (sometimes even chaotic) behaviour (Goodwine and Stépán, 2000; Le Saux et al., 2005; Schwab and Meijaard, 1999; Stépán, 1991, 2002; Takács et al., 2008). However, feed-back linearisation based controllers can be constructed for these nonlinear systems to suppress the vibrations (Goodwine and Zefran, 2002).

In this study, we consider the case when the wheel is pulled by a caster fixed to a cart of constant velocity. The lateral deformations of the tyre are modelled by the exact stretched string model. The tyre-ground contact is described by a contact line. We assume that each contact point sticks to the ground that results in a nonholonomic constraint expressed by a first-order partial differential equation (PDE). We also assume that the deformation decays exponentially outside the contact region with a characteristic relaxation

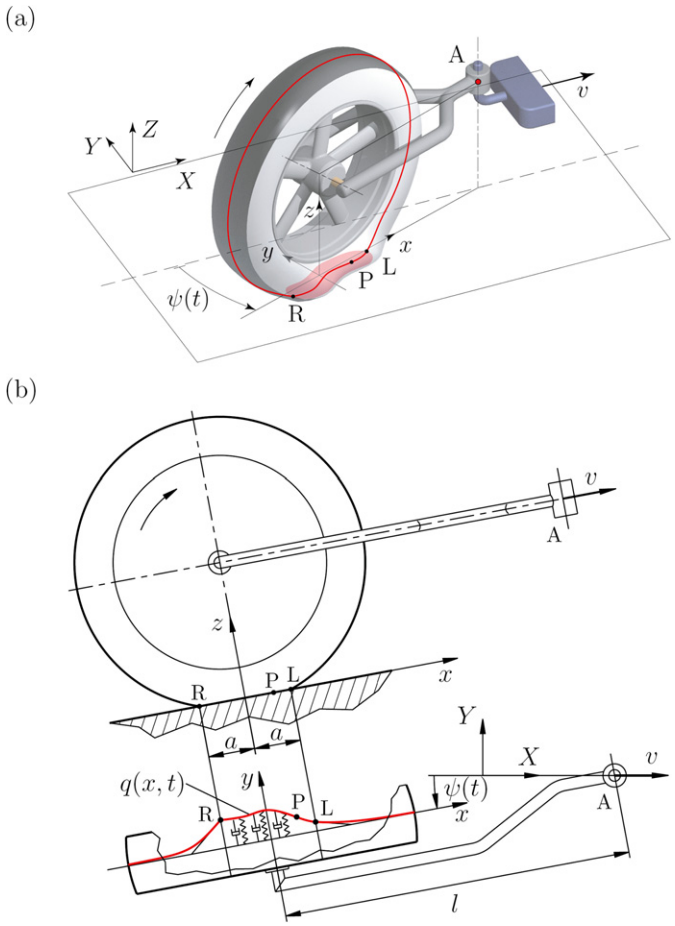

Fig. 1. Model of a towed wheel with elastic tyre. Panel (a) shows the 3-dimensional view of the wheel while panel (b) depicts the side and top view of the wheel. The deformed central line of the tyre is shown in both panels. This forms the contact line between the points L and R where the tyre is connected to the ground. The (x, y, z) coordinate system is fixed to the caster while the (X, Y, Z) coordinate system is fixed to the ground.

length. With the appropriate choice of the boundary conditions, the relaxation length of the tyre is taken into account among other conventional tyre parameters like the specific stiffness and damping. The Newtonian equation of motion becomes a second order integro differential equation (IDE). Assuming travelling wave solutions of the deformation allows us to transform the PDE-IDE system into a delay differential equation (DDE) with *distributed delay*. Here, the delay is the time needed for the leading point L of the contact line to travel backward (relative to the caster) to the actual contact point P (see Fig. 1). The linear stability investigation of the DDE shows that the stationary rolling motion may lose its stability via co-dimension one or co-dimension two Hopf bifurcations as the parameters (like the towing speed and the caster length) are varied. Consequently, self-excited periodic and quasi-periodic oscillations can appear. The stability chart in the plane of the above parameters is determined analytically and checked by numerical simulations and laboratory experiments.

2. Mechanical model

Consider the simple model of a towed wheel with elastic tyre in Fig. 1. The wheel is pulled by a caster, and the suspension point A of the caster is towed with a constant velocity v. The length of the caster is l and the tyre-ground contact length is $2a$. We consider the suspension system to be rigid and use the *exact stretched string model* of the tyre.

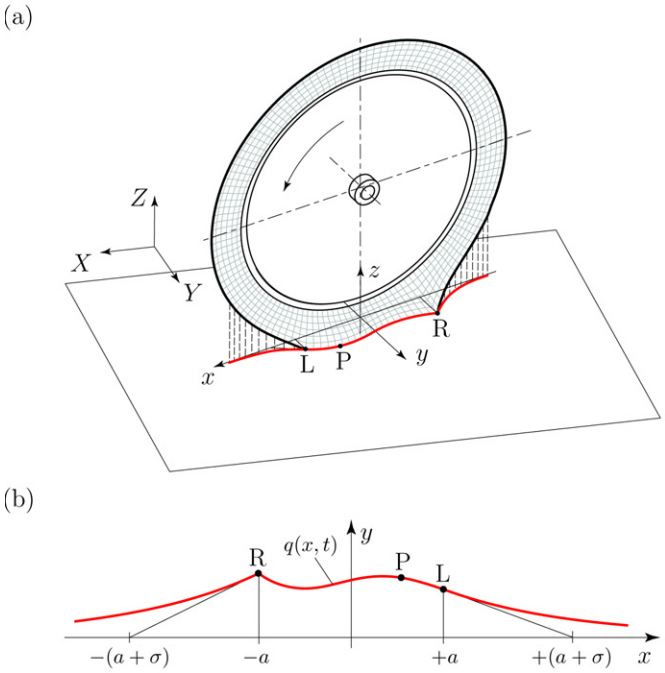

Fig. 2. Stretched string tyre model. The deformation of the central line of the tyre is shown in 3 dimension in panel (a) and projected to the ground, i.e., to the (x, y)-plane in panel (b). The relaxation length σ is identified corresponding to formula (1).

One of the chosen state variables is clearly the caster angle ψ of rotation about the vertical axis. In accordance with the stretched string model, the tyre-ground contact patch is approximated by the contact line, i.e., by the deformed central line of the tyre between the leading point L and the rear point R (see Fig. 1). Note that the deformation of the tyre outside the contact line is also described by the deformation of its central line. The lateral deformation $q(x,\cdot)$ of the central line is described in the coordinate system (x, y, z) fixed to the caster as shown in Figs. 1 and 2. This is a state variable distributed along the contact line $x \in [-a, +a]$, while it is defined by the exponentially decaying functions

$$q(x,t) = \begin{cases} q(a,t)\mathrm{e}^{-(x-a)/\sigma}, & \text{if } x \in [a,\infty), \\ q(-a,t)\mathrm{e}^{(x+a)/\sigma}, & \text{if } x \in (-\infty,-a], \end{cases} \tag{1}$$

before the leading point L and behind the rear point R. The tyre parameter σ is called the *relaxation length* (see Fig. 2(b)). This is considered to be small relative to the wheel diameter, so the theoretical extension $x \in (-\infty, +\infty)$ is an acceptable standard approximation (Pacejka, 2002; von Schlippe and Dietrich, 1941; Segel, 1966). For general theory of deformation of strings see Kármán and von Biot (1940), and for derivation of the equations of motion for moving continua see Wickert and Mote (1990).

Rolling without sliding means a nonholonomic constraint with respect to the state variables ψ and $q(x,\cdot)$ which is formulated as follows. In the ground-fixed coordinate system (X, Y, Z), the position vector of a contact point P is given as

$$\begin{bmatrix} X(x,t) \\ Y(x,t) \end{bmatrix} = \begin{bmatrix} vt - (l-x)\cos\psi(t) - q(x,t)\sin\psi(t) \\ -(l-x)\sin\psi(t) + q(x,t)\cos\psi(t) \end{bmatrix} \tag{2}$$

for $x \in [-a, a]$. (The trivial condition $Z(x,t) \equiv 0$ is not spelled out here since the vertical dynamics are neglected.) Since point P sticks to the ground, its velocity col$[\frac{\mathrm{d}X}{\mathrm{d}t}\ \frac{\mathrm{d}Y}{\mathrm{d}t}]$ is zero, that yields

$$\begin{cases} \frac{\mathrm{d}}{\mathrm{d}t}q(x,t) = v\sin\psi(t) + (l-x)\dot\psi(t), \\ \dot x = -v\cos\psi(t) + q(x,t)\dot\psi(t), \end{cases} \tag{3}$$

with

$$\frac{\mathrm{d}}{\mathrm{d}t}q(x,t) = \dot q(x,t) + q'(x,t)\dot x, \tag{4}$$

for $x \in [-a, a]$. Here $\frac{\mathrm{d}}{\mathrm{d}t}$ refers to total differentiation with respect to time t while dot and prime refer to partial differentiation with respect to time t and space x. By eliminating $\dot x$, we obtain the constraining equation for the state variables in the form of a first-order scalar partial differential equation (PDE)

$$\begin{aligned} \dot q(x,t) = {} & v\sin\psi(t) + (l-x)\dot\psi(t) \\ & + q'(x,t)\big(v\cos\psi(t) - q(x,t)\dot\psi(t)\big), \quad x \in [-a,a]. \end{aligned} \tag{5}$$

We assume that the deformation $q(x,t)$ is continuously differentiable at the leading point L which is often referred to as 'no kink at L' condition (Pacejka, 1966). This provides the mixed boundary condition

$$q'(a,t) = -\frac{q(a,t)}{\sigma} \tag{6}$$

for the PDE (5) in accordance with the exponential decay of deformation in (1) in front of the leading point L.

The equation of motion of the wheel can be given as an integro-differential equation (IDE)

$$J_A\ddot\psi(t) = -k\int_{-\infty}^{\infty}(l-x)q(x,t)\,\mathrm{d}x - b\int_{-\infty}^{\infty}(l-x)\frac{\mathrm{d}}{\mathrm{d}t}q(x,t)\,\mathrm{d}x, \tag{7}$$

where J_A is the mass moment of inertia of the wheel and the caster together with respect to the z axis at the king pin A, while k and b stand for the lateral stiffness and damping of the tyre per unit length, respectively. To simplify the model, the quantities k and b are considered to be constant even outside the contact region where the deformation of the wheel central line is projected to the ground as in Fig. 2 (even though these are constant rather along the circumference). Thus, the towed wheel model is given by the coupled PDE-IDE system (5), (7) when considering the approximation (1) and the boundary condition (6).

3. Travelling wave solutions and time delay

Let $\tau(x)$ denote the time needed for a tyre particle located at the leading point L to travel backward (relative to the caster) to the actual point P characterised by the coordinate x. With this delay, we can describe a travelling wave solution as

$$\begin{bmatrix} X(x,t) \\ Y(x,t) \end{bmatrix} = \begin{bmatrix} X(a,t-\tau(x)) \\ Y(a,t-\tau(x)) \end{bmatrix}, \tag{8}$$

which simply expresses the fact that the tyre particles once fixed to the ground remain fixed there, while the caster travels ahead above them. With the help of (2), the travelling wave (8) can be transformed into the form

$$\begin{cases} l - x = v\tau\cos\psi(t) + (l-a)\cos(\psi(t) - \psi(t-\tau)) \\ \qquad - q(a,t-\tau)\sin(\psi(t) - \psi(t-\tau)), \\ q(x,t) = v\tau\sin\psi(t) + (l-a)\sin(\psi(t) - \psi(t-\tau)) \\ \qquad + q(a,t-\tau)\cos(\psi(t) - \psi(t-\tau)), \end{cases} \tag{9}$$

which is still implicit due to the fact that $\tau(x)$ cannot be expressed in closed form. However, differentiating the first equation in (9) with respect to τ, we obtain

$$\begin{aligned} \frac{\mathrm{d}x}{\mathrm{d}\tau} = {} & -v\cos\psi(t) + (l-a)\dot\psi(t-\tau)\sin\big(\psi(t) - \psi(t-\tau)\big) \\ & - \dot q(a,t-\tau)\sin\big(\psi(t) - \psi(t-\tau)\big) \\ & + q(a,t-\tau)\dot\psi(t-\tau)\cos\big(\psi(t) - \psi(t-\tau)\big). \end{aligned} \tag{10}$$

Now, one may substitute (1), (3), (9) into (7) and use the change of variables x and τ (integration by substitution) based on (10). The resulting retarded functional differential equation (RFDE) contains the time dependent caster angle $\psi(t)$ and its delayed values $\psi(t-\tau)$, and the time dependent leading point lateral deformation $q(a,t)$ and its delayed values $q(a,t-\tau)$. The constraining equation (5) with its boundary condition (6) provides an ordinary differential equation (ODE) for the leading point lateral deformation:

$$\dot{q}(a,t) = v\sin\psi(t) + (l-a)\dot{\psi}(t) - \frac{v}{\sigma}q(a,t)\cos\psi(t) + \frac{1}{\sigma}q^2(a,t)\dot{\psi}(t). \tag{11}$$

The above described nonlinear RFDE-ODE system was given explicitly for the special case of zero relaxation length ($\sigma = 0$) and zero damping ($b = 0$) in Stépán (1998). For nonzero σ and b the explicit linearised equations are given in the next section.

Pacejka's creep force/moment model also uses the leading point lateral deformation as state variable, but instead of the travelling wave solution along the contact line, it uses the stationary lateral deformation obtained at constant drift angle ψ (Pacejka, 1966). This way, one obtains a three dimensional nonlinear ODE instead of the infinite dimensional nonlinear RFDE-ODE, but loses the dynamics within the contact region, which may be important in certain parameter domains as identified later.

4. Small oscillations around stationary rolling

The stationary rolling motion of the wheel is described by the trivial solution

$$\psi(t) \equiv 0, \quad q(x,t) \equiv 0, \quad x \in (-\infty, +\infty). \tag{12}$$

Small shimmy oscillations around the stationary rolling can be described by the linearisation of the governing equations (7), (9)–(11):

$$\begin{aligned} J_A\ddot{\psi}(t) = &-k\int_{-a}^{a}(l-x)\left(q(x,t) + \frac{b}{k}\frac{\mathrm{d}}{\mathrm{d}t}q(x,t)\right)\mathrm{d}x \\ &- k\sigma(l-a-\sigma)\left(q(a,t) + \frac{b}{k}\left(\dot{q}(a,t) + \frac{v}{\sigma}q(a,t)\right)\right) \\ &- k\sigma(l+a+\sigma)\left(q(-a,t) \right. \\ &\left. + \frac{b}{k}\left(\dot{q}(-a,t) - \frac{v}{\sigma}q(-a,t)\right)\right), \end{aligned} \tag{13}$$

$$\begin{cases} l-x = v\tau + l - a \Rightarrow \tau(x) = \frac{a-x}{v}, \\ q(x,t) = (v\tau + l - a)\psi(t) - (l-a)\psi(t-\tau) + q(a,t-\tau), \end{cases} \tag{14}$$

$$\frac{\mathrm{d}x}{\mathrm{d}\tau} = -v, \tag{15}$$

$$\dot{q}(a,t) = v\psi(t) + (l-a)\dot{\psi}(t) - \frac{v}{\sigma}q(a,t). \tag{16}$$

In (13) the integrals over the intervals $(-\infty, -a]$, and $[a, \infty)$ are calculated in closed form by using the exponential decay functions in (1), while the remaining $\frac{\mathrm{d}}{\mathrm{d}t}q(x,t)$ can be obtained from the linearisation of (3). The second equation in (14) means that the lateral deformation $q(x,t)$ can be expressed by the present and delayed values of the caster angle ψ and the leading point lateral deformation $q(a,\cdot)$.

In particular, considering the first equation in (14) at the rear point R, we obtain

$$x = -a \Rightarrow \tau(-a) = \frac{2a}{v}. \tag{17}$$

and so the second equation in (14) at the rear point R gives

$$q(-a,t) = (l+a)\psi(t) - (l-a)\psi\left(t - \frac{2a}{v}\right) + q\left(a, t - \frac{2a}{v}\right). \tag{18}$$

After substituting (14), (15), (17), (18) into the IDE (13) and dividing the equation with the mass moment of inertia J_A, we obtain the form

$$\begin{aligned} &\ddot{\psi}(t) + 2\zeta\omega_n\dot{\psi}(t) + \omega_n^2\psi(t) \\ &= \frac{kv}{J_A}\int_0^{2a/v}(l-a+v\tau)p(t-\tau)\,\mathrm{d}\tau \\ &\quad + \frac{k\sigma}{J_A}(l-a-\sigma)\left(p(t) + \frac{2\zeta}{\omega_n}\left(\dot{p}(t) + \frac{v}{\sigma}p(t)\right)\right) \\ &\quad + \frac{k\sigma}{J_A}(l+a+\sigma)\left(p\left(t-\frac{2a}{v}\right)\right. \\ &\quad \left. + \frac{2\zeta}{\omega_n}\left(\dot{p}\left(t-\frac{2a}{v}\right) - \frac{v}{\sigma}p\left(t-\frac{2a}{v}\right)\right)\right) \\ &\quad + \frac{bv}{J_A}2l(a+\sigma)\psi(t), \end{aligned} \tag{19}$$

where we temporarily introduced the new notation

$$p(t) = (l-a)\psi(t) - q(a,t) \tag{20}$$

for the absolute position Y of the leading point L to shorten the expression. The constants

$$\omega_n = \sqrt{\frac{2k}{J_A}\left(a\left(l^2 + a^2/3\right) + \sigma\left(l^2 + a^2 + a\sigma\right)\right)} \quad \text{and}$$

$$\zeta = \frac{\omega_n}{2}\frac{b}{k} \tag{21}$$

are the undamped natural angular frequency and the damping ratio of the steady wheel ($v = 0$), respectively.

5. Rescaling

Let us rescale the time as

$$T := \frac{v}{2a}t, \tag{22}$$

define the new integration variable by

$$\vartheta := -\frac{v}{2a}\tau, \tag{23}$$

and the dimensionless leading point lateral deformation by

$$Q(T) := \frac{1}{a}q(a,T). \tag{24}$$

Now, using dot as partial differentiation with respect to the rescaled time T, we can define the dimensionless angular velocity as

$$\Omega(T) := \dot{\psi}(T). \tag{25}$$

Furthermore, the dimensionless towing speed V, the dimensionless caster length L and the dimensionless relaxation length Σ are given by

$$V := \frac{1}{\omega_n}\frac{v}{2a}, \quad L := \frac{l}{a}, \quad \Sigma := \frac{\sigma}{a}, \tag{26}$$

respectively.

Using definitions (22)–(26), the ODE (16) and the IDE (19), (20) provide a 3-dimensional system of first-order DDEs:

$$\begin{bmatrix}\dot\psi(T)\\ \dot\Omega(T)\\ \dot Q(T)\end{bmatrix}=\begin{bmatrix}0 & 1 & 0\\ -\frac{1}{V^2}+c_1c_2 & -\frac{2\zeta}{V} & -c_2\frac{\Sigma}{2}(L-1-\Sigma)\\ 2 & L-1 & -\frac{2}{\Sigma}\end{bmatrix}\begin{bmatrix}\psi(T)\\ \Omega(T)\\ Q(T)\end{bmatrix}$$
$$+c_2\int_{-1}^{0}(L-1-2\vartheta)\begin{bmatrix}0&0&0\\ L-1&0&-1\\ 0&0&0\end{bmatrix}\begin{bmatrix}\psi(T+\vartheta)\\ \Omega(T+\vartheta)\\ Q(T+\vartheta)\end{bmatrix}\mathrm{d}\vartheta$$
$$+\frac{c_2}{2}(L+1+\Sigma)\times\begin{bmatrix}0&0&0\\ (\Sigma-4\zeta V)(L-1)-4\Sigma\zeta V&0&8\zeta V-\Sigma\\ 0&0&0\end{bmatrix}\times\begin{bmatrix}\psi(T-1)\\ \Omega(T-1)\\ Q(T-1)\end{bmatrix},\tag{27}$$

where

$$c_1=\frac{\Sigma}{2}(L-1-\Sigma)(L-1)+2\zeta V\left(L^2+(1+\Sigma)^2\right),$$
$$c_2=\frac{1}{V^2}\frac{1}{L^2+1/3+\Sigma(L^2+1+\Sigma)}.\tag{28}$$

6. Stability investigation

The stationary rolling motion (12) is now represented by the trivial solution

$$\begin{bmatrix}\psi(T)\\ \Omega(T)\\ Q(T)\end{bmatrix}\equiv\mathbf{0}\tag{29}$$

of the linearised equation of motion (27). The Laplace transformation of (27) or the substitution of the trial solution

$$\begin{bmatrix}\psi(T)\\ \Omega(T)\\ Q(T)\end{bmatrix}=\mathbf{K}\mathrm{e}^{\lambda T},\quad \mathbf{K}\in\mathbb{C}^3,\lambda\in\mathbb{C}\tag{30}$$

leads to the characteristic function

$$D(\lambda;\mu)=\Sigma V^2\lambda^3+2V(V+\Sigma\zeta)\lambda^2+(\Sigma+4\zeta V)\lambda+2$$
$$-\frac{L-1-\Sigma}{L^2+1/3+\Sigma(L^2+1+\Sigma)}\times\left\{\frac{2}{\lambda^2}\left((L-1)\lambda+2-\left((L+1)\lambda+2\right)\mathrm{e}^{-\lambda}\right)\right.$$
$$+\frac{4\zeta VL(1+\Sigma)(2+\Sigma\lambda)}{L-1-\Sigma}$$
$$+(L-1-\Sigma)(2\Sigma\zeta V\lambda+\Sigma+4\zeta V)$$
$$\left.+(L+1+\Sigma)(2\Sigma\zeta V\lambda+\Sigma-4\zeta V)\mathrm{e}^{-\lambda}\right\},\tag{31}$$

where $\mu\in\mathbb{R}^4$ represents the dimensionless parameters ordered in a vector

$$\mu=\mathrm{col}[V\quad L\quad \Sigma\quad \zeta].\tag{32}$$

Generally, Eq. (31) has infinitely many complex zeros for the characteristic exponents (characteristic roots) λ, but only a finite number of these may be situated in the right-half complex plane. The stationary rolling (12), (29) is asymptotically stable if and only if all the infinitely many characteristic exponents are situated in the left-half complex plane (Stépán, 1989).

At the limit of stability, bifurcation can take place in the corresponding nonlinear system when characteristic roots are located at the imaginary axis for some critical values μ_{cr} of the parameter vector. It is easy to see, that the critical characteristic root cannot be the zero since it does not satisfy the characteristic equation for any parameter values, i.e., $D(0,\mu)\neq 0$. This means that only Hopf bifurcation can occur at μ_{cr} when a pair of pure imaginary complex conjugate characteristic exponents

$$\lambda_{1,2}(\mu_{\mathrm{cr}})=\pm\mathrm{i}\omega,\quad \omega\in\mathbb{R}^+,\tag{33}$$

satisfy (31) with the dimensionless angular frequency ω. Due to this bifurcation, self-excited vibrations may appear in the corresponding nonlinear system around the stationary rolling motion with dimensional frequency $f=\omega v/(4a\pi)=\omega V\omega_{\mathrm{n}}/(2\pi)$ in Hertz. Consequently, travelling waves propagate backward along the contact line with dimensional wave length $v/f=4a\pi/\omega$.

The stability boundaries are determined in the parameter space by the substitution of the characteristic exponent $\lambda_1=\mathrm{i}\omega$ into (31) and by the separation of the real and imaginary parts:

$$\mathrm{Re}\,D(\mathrm{i}\omega;\mu_{\mathrm{cr}})=0,\qquad \mathrm{Im}\,D(\mathrm{i}\omega;\mu_{\mathrm{cr}})=0.\tag{34}$$

In the 4-dimensional parameter space $\mu\in\mathbb{R}^4$, these formulae describe stability boundaries (3-dimensional hypersurfaces) parameterised by the dimensionless angular frequency $\omega\in\mathbb{R}^+$. Fixing 2 of the 4 parameters, we obtain stability boundary curves in a parameter plane. In particular, we fix the dimensionless relaxation length Σ and the damping ratio ζ for different values, and construct stability boundary curves in the plane of the dimensionless towing speed V and the dimensionless caster length L. To decide whether a certain region bounded by the intricate structure of stability curves is stable or not, we use the stability criteria derived in Stépán (1989). The stable parameter domains are shaded in the stability charts plotted in the (V,L)-plane in Fig. 3 for different values of Σ for the undamped system ($\zeta=0$). Notice that there exists a boundary at $L=1+\Sigma$ for any Σ, and for large V the system is stable above this boundary and unstable below. Fig. 4 shows the stability charts in the (V,L)-plane for a measured value of Σ (see Fig. 7 later) when ζ is increased. It can be observed that the unstable 'lenses' gradually shrink and disappear as the damping is increased and only the monotone increasing stability curve persist for large damping ($\zeta>0.035$). This curve saturates at $L=1+\Sigma$ for large V.

Where the stability boundary curves intersect each other, two pairs of pure imaginary characteristic exponents $\pm\mathrm{i}\omega_1$ and $\pm\mathrm{i}\omega_2$ co-exist with two dimensionless angular frequencies ω_1 and ω_2. This is a co-dimension two (or double) Hopf bifurcation which also arises in a similar delayed robot dynamics problem (Stépán and Haller, 1995). Due to this bifurcation quasi-periodic self-excited oscillations appear around the stationary rolling motion with dimensional frequencies $f_1=\omega_1 v/(4a\pi)=\omega_1 V\omega_{\mathrm{n}}/(2\pi)$ and $f_2=\omega_2 v/(4a\pi)=\omega_2 V\omega_{\mathrm{n}}/(2\pi)$. The corresponding 'quasi-periodic travelling waves' in the contact region possess the dimensional wave lengths $v/f_1=4a\pi/\omega_1$ and $v/f_2=4a\pi/\omega_2$.

Instead of carrying out the analytical study of co-dimension one and two Hopf bifurcations that would require the reduction of the dynamics from the infinite-dimensional state space to 2- and 4-dimensional centre manifolds, we identified typical periodic and quasi-periodic vibrations in the system by numerical simulations. These provide enough information at this stage of the research for the validation of our model by experiments.

7. Simulation of the nonlinear equations

In order to demonstrate the stability properties determined above we study the original PDE-IDE system (5), (7) with conditions (1), (6) by numerical simulation. On one hand we wish to verify that the obtained linear stability diagrams are correct. On the other hand we would like to obtain information about the appearing nonlinear oscillations when the stationary rolling motion is linearly unstable.

We fix the dimensional parameters a, σ, k and b as in Table 1 and vary v, l and J_{A} such that ω_{n} is kept constant (see (21)).

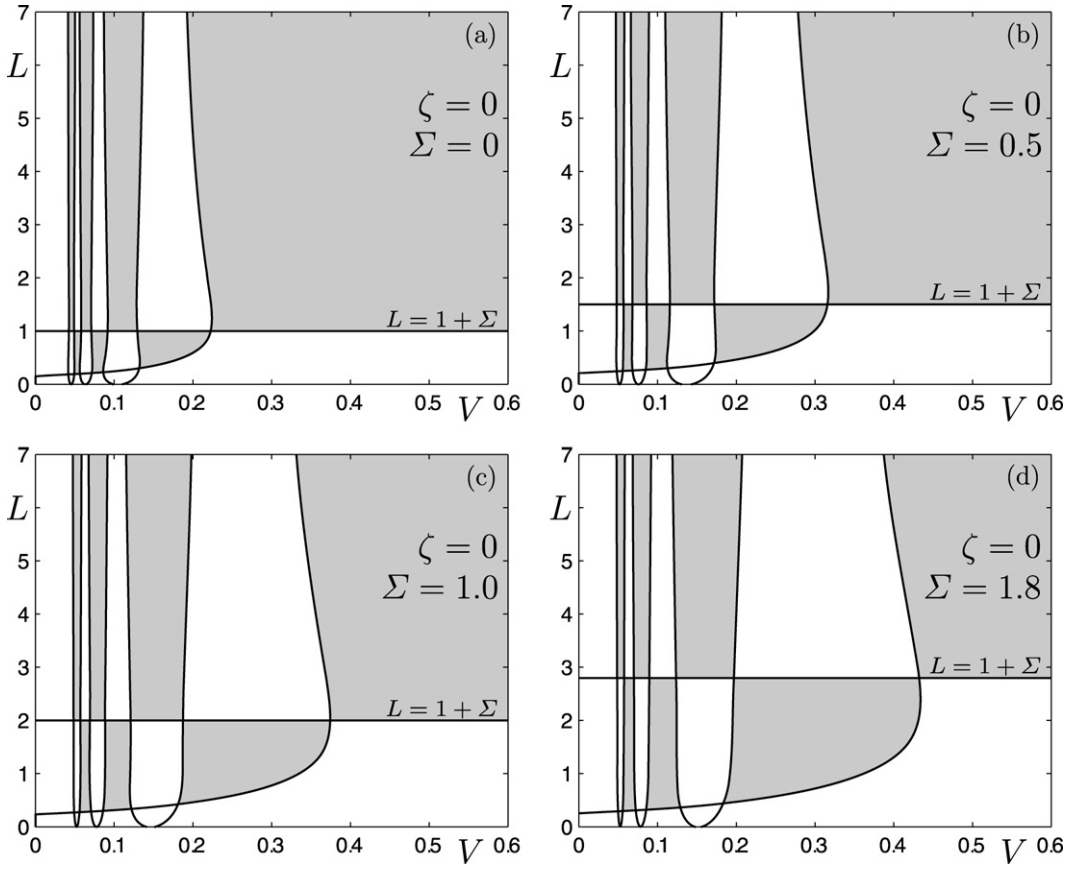

Fig. 3. Stability charts in the (V, L)-plane for the undamped system ($\zeta = 0$) for different values of the dimensionless relaxation length Σ. Stable regions are shaded. The stability boundary curves refer to Hopf bifurcations, their intersections refer to co-dimension two Hopf bifurcations.

Table 1
The experimentally identified dimensional parameters and their dimensionless counterparts; see formulae (21) and (26).

Dimensional parameters	Dimensionless parameters
$a = 0.04$ [m]	$\Sigma = 1.8$
$\sigma = 0.072$ [m]	
$k = 53506$ [N/m^2]	$\zeta = 0.02$
$b = 140$ [Ns/m^2]	
$\omega_n = 15.29$ [rad/s]	
$f_n = 2.43$ [Hz]	

Consequently, the dimensionless parameters Σ and ζ keep their values shown in Table 1 while V and L are varied (see (26)). This means that we consider the stability diagram in Fig. 4(c) where the points A–D are marked by crosses. We run the simulations using the parameters at these points. In each of the pairs A–C and B–D the points are separated by a Hopf curve such that one point lies in the stable (shaded) regime while the other in the unstable (white) regime. Consequently, qualitatively different behaviour is expected for the two points of each pair.

To integrate the PDE-IDE system (5), (7) we use the Lax–Wendroff method (Lax and Wendroff, 1960) which provides second order accuracy in time. Note that for the IDE component this method is effectively the same as the 2nd order Runge–Kutta method. The number of spatial mesh points was 400. Furthermore, we consider the initial condition

$$\psi(0) = 0, \qquad \dot{\psi}(0) = w,$$
$$q(0, x) \equiv 0, \qquad \dot{q}(0, x) = (l - x)w, \qquad x \in [-a, a], \tag{35}$$

with constant $w = 1$ [rad/s]. This corresponds to applying a lateral impact to the stationary rolling wheel at $t = 0$.

The obtained results are shown in Fig. 5. In each panel the time history for the caster angle $\psi(t)$ is shown together with the spatial distribution of the lateral deformation $q^*(x) = q(x, t^*)$ at the chosen time t^*. Fig. 5 (a) and (b) show the cases A and B where the stationary rolling motion is linearly stable, that is, small perturbations around this motion decay in time. Observe that the small amplitude oscillations/waves are very close to harmonic. Fig. 5 (c) and (d) show the cases C and D where the stationary rolling motion is linearly unstable, that is, small perturbations grow in time and the system approaches large-amplitude oscillations as time progresses. In case C the approached motion is periodic corresponding to a limit cycle in phase space while in case D quasi-periodic oscillations are observed which correspond to a torus in phase space. The large amplitude oscillations/waves are not harmonic anymore, but these are not realistic physically due to the large caster angles reaching even $\pi/2$. This will be further discussed in Section 8 on comparison to experimental observations.

Considering cases A and C the appearing dimensional frequency and wavelength are close to $f = \omega V \omega_n/(2\pi) = 0.93 f_n$ and $4a\pi/\omega = 3.22(2a)$, respectively, where the dimensionless angular frequency $\omega = 1.95$ is obtained from the neighbouring Hopf curve. Similarly, in cases B and D the appearing dimensional angular frequencies are close to $f_1 = \omega_1 V \omega_n/(2\pi) = 0.27 f_n$ and $f_2 = \omega_2 V \omega_n/(2\pi) = 1.03 f_n$, and the appearing wavelengths are close $4a\pi/\omega_1 = 3.85(2a)$ and $4a\pi/\omega_2 = 1.01(2a)$, respectively. Here the dimensionless angular frequencies $\omega_1 = 1.63$ and $\omega_2 = 6.20$ belong to the neighbouring co-dimension two Hopf point.

8. Experimental validation

An experimental rig has been designed and constructed to test the above time-delayed model of shimmy motion of a towed wheel

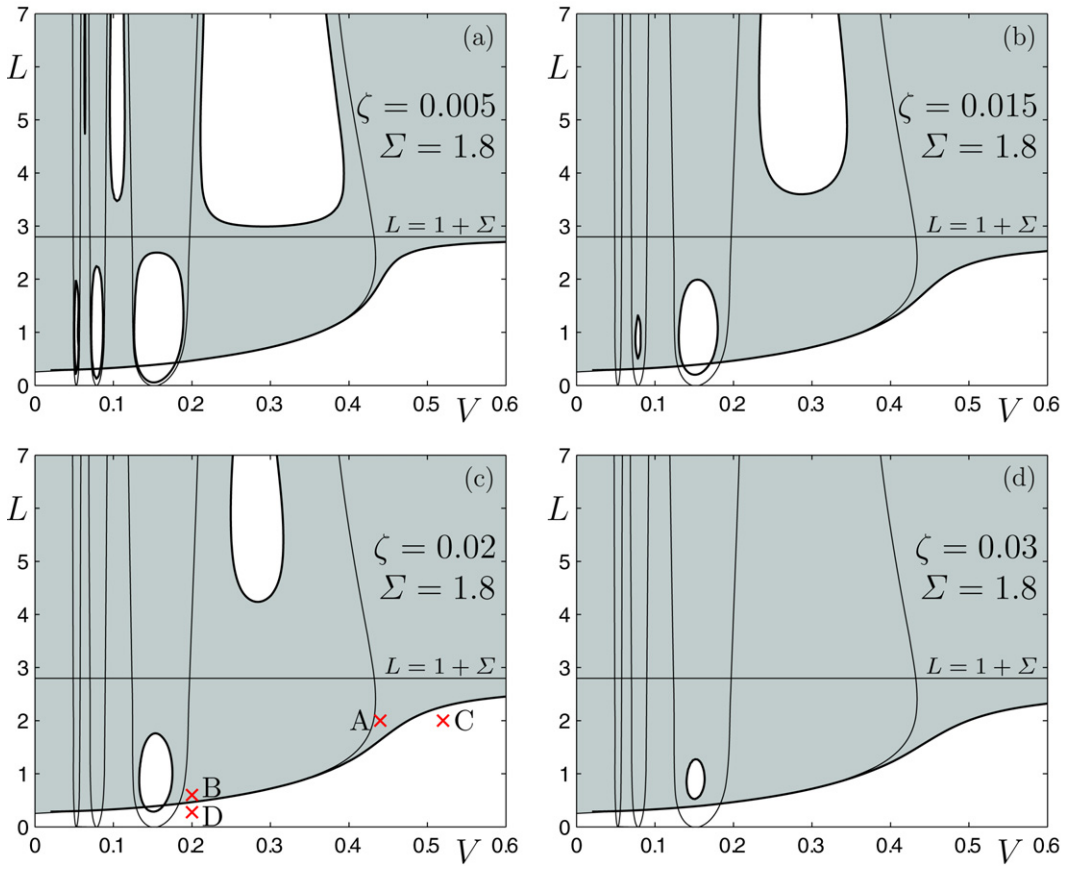

Fig. 4. Stability charts in the (V, L)-plane for different values of the damping ratio ζ with fixed dimensionless relaxation length $\Sigma = 1.8$. Stable regions are shaded. The stability boundary curves refer to Hopf bifurcations, their intersections refer to co-dimension two Hopf bifurcations. Thin curves correspond to the stability boundaries of the undamped system ($\zeta = 0$) for the same $\Sigma = 1.8$ (see Fig. 3(d)). In panel (c) the crosses A–D show the parameter values used for the numerical simulations in Fig. 5.

with elastic tyre (Takács, 2005; Takács and Stépán, 2007). The wheel was placed on a conveyor belt of variable speed as shown in Fig. 6. In order to avoid oscillations due to the elasticity of the conveyor belt, it was stiffened laterally by a steel frame which also kept the possible lateral buckling of the conveyor belt under control. The caster length and the mass moment of inertia of the structure with respect to the vertical axis at the king pin A were also adjustable. In this way, we were able to tune the natural angular frequency ω_n and the damping ratio ζ to desired values (see (21), (26)). Thus, all the necessary parameters were controlled within certain limits to identify an experimental stability chart in the plane of dimensionless towing speed V and dimensionless caster length L (for fixed dimensionless relaxation length Σ and damping ratio ζ). Since all dimensionless parameters depend on the caster length l and the contact length $2a$, the proper variation of the system parameters requires special attention.

In order to identify the numerical values of parameters, first, we fixed a certain air pressure in the pneumatic tyre, placed the wheel in a rigid frame as in Fig. 7(a) and pulled its centre point in lateral direction. Fig. 7(b) shows the enlarged (and distorted) picture of the deformed tyre in and around the contact region when a transparent plastic plate was placed at one side of the frame and the central line of the tyre was marked. This picture perfectly follows the approximation (1) of the stretched string model used in the literature (Pacejka, 2002; von Schlippe and Dietrich, 1941; Segel, 1966). We identified the contact length $2a$ and the relaxation length σ, and the obtained results are shown in Table 1.

Then the standing wheel was placed to the conveyor belt as in Fig. 6 and its centre was slightly hit in lateral direction. The time history of the acceleration of a chosen caster point was recorded. From the frequency and logarithmic decrement of the vibration signal the natural angular frequency ω_n and the damping ratio ζ can be determined. Using (21) the lateral stiffness k and lateral damping b per unit length can be calculated. The obtained results are also given in Table 1.

During the experiments, for a chosen caster length l, we increased the towing speed v step-by-step and identified the loss of stability of stationary rolling by detecting the appearance of self-excited vibrations, i.e., the shimmy. Then we repeated the same experiment for several different values of the caster length l. We managed to keep the constant value for the natural frequency f_n when the caster length l was varied: we varied the mass at the end of the caster and the mass moment of inertia J_A changed accordingly. Consequently, the damping ratio ζ and the dimensionless relaxation length Σ were also kept constant (see (21), (26)).

The experimental stability chart was transformed to the (V, L)-plane of dimensionless parameters. Fig. 8 compares this measured stability chart with the corresponding theoretical stability chart calculated from the time-delayed model for the experimentally identified parameters in Table 1 (see also the bottom part of Fig. 4(c)). This shows relatively good agreement between theory and experiment. Recall that the theoretical stability boundary saturates at $L = 1 + \Sigma$ for large V. Fig. 8 shows that the experimental stability boundary saturates to a slightly higher value of L. This suggests that one may obtain a better fit for large V by considering slightly higher value of Σ than the measured one.

In Fig. 8 we marked by a cross the point D on the experimental stability boundary which is located close to the double Hopf point (the intersection of the theoretical stability curves). This is the same point as point D in Fig. 4(c) where quasi-periodic oscil-

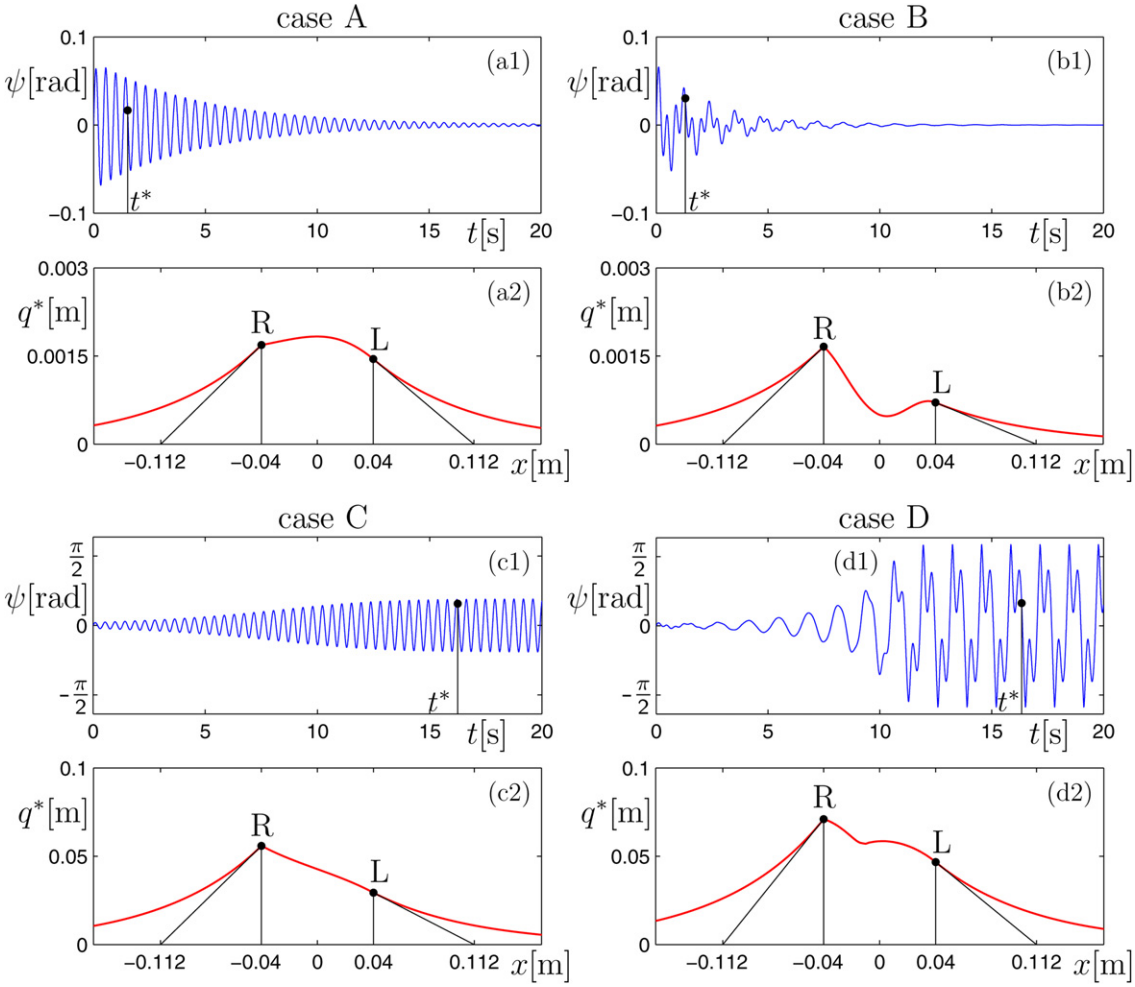

Fig. 5. Numerical simulation results for the points marked by red crosses in Fig. 4(c). In each panel the time profile for the caster angle $\psi(t)$ is shown and the spatial distribution of the lateral deformation $q^*(x) = q(x, t^*)$ is depicted at time t^*. In panels (a) and (c) the stationary rolling motion is linearly stable, while in panels (b) and (d) this motion is unstable and stable oscillating (shimmy) motions can be observed. (For interpretation of the references to color in this figure legend, the reader is referred to the web version of this article.)

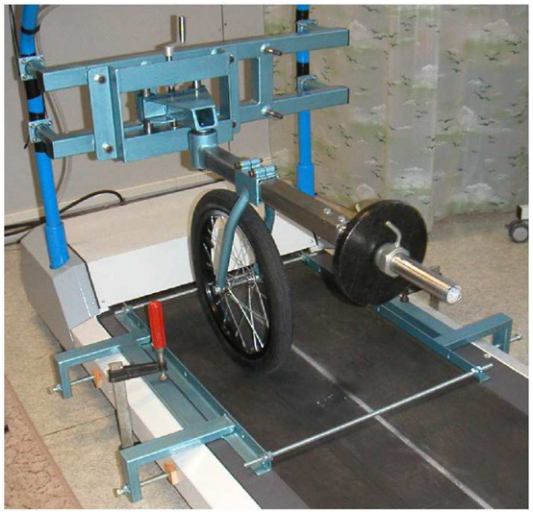

Fig. 6. The experimental rig on the stiffened conveyor belt.

lations were found by numerical simulation as shown in Fig. 5(d). Our measurements confirm these observations as quasi-periodic vibrations appear in the experiments, too. However, we found that the amplitude of oscillations in the experiments is lower than suggested by simulations. These deviations are due to the shortcoming of our model that the tyre sticks to the ground even for very large lateral deformations, while in reality sliding usually occurs at the rear part of the contact region. Involving this dissipative effect one might be able to obtain better agreement between simulations and measurements. More details about this analysis can be found in Takács and Stépán (2007).

9. Conclusion and discussions

A low degree-of-freedom model of the shimmying wheel with elastic tyre was investigated. The no-slip kinematic constraint along tyre-ground contact region was described by a nonlinear partial differential equation (PDE) which was coupled to an integro-differential equation (IDE) of wheel motion. Considering the relaxation of tyre deformation around the contact region provided a boundary condition for the coupled nonlinear PDE-IDE system.

The equations were linearised about the stationary rolling motion. Using travelling wave solutions the linearised PDE-IDE was transformed into a 3-dimensional linear system of delay differential equations (DDEs). In this way, stability charts were constructed analytically in the plane of the towing speed and caster length for certain damping ratio and relaxation length parameters. Crossing the stability boundaries in the stability chart, Hopf bifurcations take place leading to self-excited vibrations in the corresponding nonlinear PDE-IDE system. The appearing periodic and quasi-periodic oscillations were found by numerical simulations

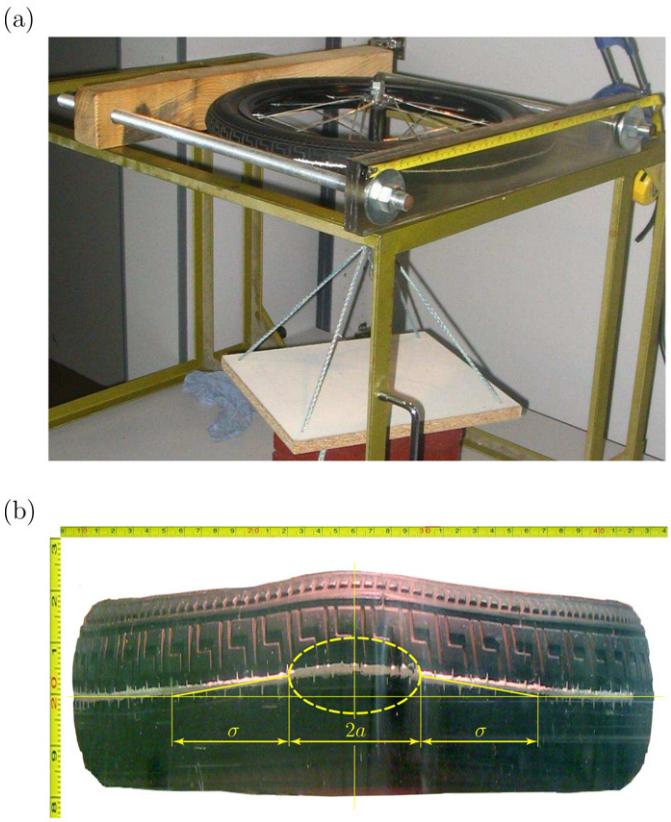

Fig. 7. Measuring tyre parameters. Panel (a) shows the static lateral load on the framed wheel. Panel (b) shows the measurements of contact length $2a$ and relaxation length σ of the tyre contacting a transparent plastic plate.

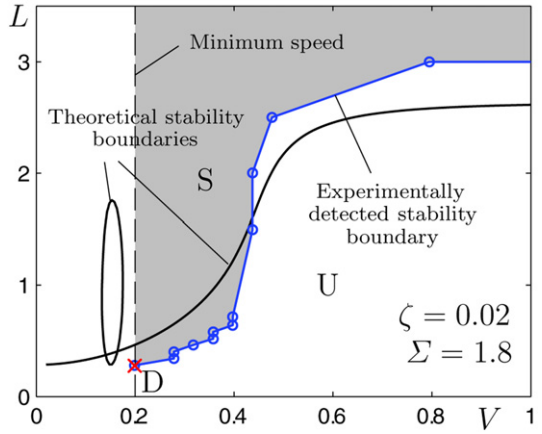

Fig. 8. Figure compares the experimentally identified stability boundary (piecewise smooth line with circles) with the theoretical stability boundaries (smooth lines) on the (V, L)-plane. The experimentally identified stable region is shaded. For parameter values at the point D (marked by cross) quasi-periodic oscillations were found by numerical simulation and by experiment, too.

and the stability chart was confirmed numerically. A constructed experimental rig allowed to detect the periodic and quasi-periodic oscillations experimentally and to determine an experimental stability chart having a reasonable good match to the theoretical one.

The experimental stability chart confirmed the importance of the nonzero relaxation length. In previous experimental studies where zero relaxation length was considered (Takács, 2005; Takács and Stépán, 2007), the results showed large deviation from theoretical predictions for large towing speed and long caster. The appearance of quasi-periodic self-excited oscillations at low towing speed and short caster also validates the delayed shimmy model. To explain these oscillations it is essential to describe appropriately the 'motion of the contact line'. Single degree-of-freedom models with creep force approximation cannot predict quasi-periodic behaviour because they omit the dynamics within the contact region. Nevertheless, whether a towing speed is considered to be large or small depends on the natural frequency of the system, and also on the length of the contact patch as it is expressed by the dimensionless towing speed.

Note that the proper bifurcation analysis of the nonlinear system has not been carried out yet. This can be very complicated in the studied infinite dimensional system in particular in the vicinity of the double Hopf bifurcation points. In order to resolve this problem one needs to consider the nonlinear terms and use either normal form calculations (Campbell and Bélair, 1995; Orosz, 2004) or numerical continuation techniques (Engelborghs et al., 2001; Szalai et al., 2006). For example, carrying out these calculations for nonlinear point contact models with rigid tyre, strong subcritical behaviour was found (Stépán, 1991; Takács et al., 2008). Subcriticality results in small-amplitude unstable oscillations around the stable stationary rolling and also predicts bistability between stationary rolling and large-amplitude oscillations.

Further development of our model is possible by involving sliding of the tyre at the rear part of the contact region. The appearing friction force dissipates energy and may allow us to have a better match between simulations and experiments (Takács and Stépán, 2007). However, allowing the wheel to slide may also lead to very complicated (e.g., chaotic) large-amplitude vibrations in some parameter regimes (Stépán, 1991; Takács et al., 2008). We consider these problems for future research directions.

Acknowledgements

The research of D.T. and G.S. was supported by the Hungarian National Science Foundation under grant no. OTKA T043368. G.O. acknowledges the discussions with Andrew Gilbert on numerical methods for PDEs. The authors thank the reviewers for the detailed and useful comments.

References

Böhm, F., 1989. Model for the radial tire for high frequent rolling-contact. Vehicle System Dynamics 18 (Suppl.), 72–83.
Campbell, S.A., Bélair, J., 1995. Analytical and symbolically-assisted investigations of Hopf bifurcations in delay-differential equations. Canadian Applied Mathematics Quarterly 3 (2), 137–154.
Chang, Y.P., El-Gindy, M., Streit, D.A., 2004. Literature survey of transient dynamic response tyre models. International Journal of Vehicle Design 34 (4), 354–386.
Collins, R.L., 1971. Theories on mechanics of tyres and their application to shimmy analysis. Journal of Aircraft 8 (4), 271–277.
Engelborghs, K., Luzyanina, T., Samaey, G., 2001. DDE-BIFTOOL v. 2.00: A Matlab package for bifurcation analysis of delay differential equations. Tech. Rep. TW-330, Department of Computer Science, Katholieke Universiteit Leuven, Belgium, http://www.cs.kuleuven.ac.be/~koen/delay/ddebiftool.shtml.
Fratila, D., Darling, J., 1996. Simulation of coupled car and caravan handling behaviour. Vehicle System Dynamics 26 (6), 397–429.
Goodwine, B., Stépán, G., 2000. Controlling unstable rolling phenomena. Journal of Vibration and Control 6 (1), 137–158.
Goodwine, B., Zefran, M., 2002. Feedback stabilization of a class of unstable nonholonomic systems. Journal of Dynamic Systems Measurement and Control, Transactions of the ASME 124 (1), 221–230.
Kalker, J.J., 1991. Wheel rail rolling-contact theory. Wear 144 (1–2), 243–261.
Kármán, T., von Biot, M.A., 1940. Mathematical Methods in Engineering. McGraw-Hill Book Company, Inc., New York.
Lax, P.D., Wendroff, B., 1960. Systems of conservation laws. Communications on Pure and Applied Mathematics 13 (2), 217–237.
Le Saux, C., Leine, R.I., Glocker, C., 2005. Dynamics of a rolling disk in the presence of dry friction. Journal of Nonlinear Science 15 (1), 27–61.
Moreland, W.J., 1954. The story of shimmy. Journal of the Aeronautical Sciences 21 (12), 793–808.
Orosz, G., 2004. Hopf bifurcation calculations in delayed systems. Periodica Polytechnica 48 (2), 189–200.

Pacejka, H.B., 1966. The wheel shimmy phenomenon. Ph.D. thesis, Technical University of Delft, The Netherlands.

Pacejka, H.B., 2002. Tyre and Vehicle Dynamics. Elsevier Butterworth-Heinemann, Oxford.

Schiehlen, W., 2006. Computational dynamics: theory and applications of multibody systems. European Journal of Mechanics A/Solids 25 (4), 566–594.

Schlippe, B., Dietrich, R., 1941. Das Flattern eines bepneuten Rades (Shimmying of a pneumatic wheel). In: Bericht 140 der Lilienthal-Gesellschaft für Luftfahrtforschung. pp. 35–45, 63–66. English translation is available in NACA Technical Memorandum 1365, pp. 125–166, 217–228, 1954.

Schwab, A.L., Meijaard, J.P., 1999. Dynamics of flexible multibody systems having rolling contact: application of the wheel element to the dynamics of road vehicles. Vehicle System Dynamics 33 (Suppl.), 338–349.

Segel, L., 1966. Force and moment response of pneumatic tires to lateral motion inputs. Journal of Engineering for Industry, Transactions of the ASME 88B (1), 37–44.

Sharp, R.S., Evangelou, S., Limebeer, D.J.N., 2004. Advances in the modelling of motorcycle dynamics. Multibody System Dynamics 12 (3), 251–283.

Stépán, G., 1989. Retarded Dynamical Systems: Stability and Characteristic Functions. Pitman Research Notes in Mathematics, vol. 210. Longman, Essex, England.

Stépán, G., 1991. Chaotic motion of wheels. Vehicle System Dynamics 20 (6), 341–351.

Stépán, G., 1998. Delay, nonlinear oscillations and shimmying wheels. In: Moon, F.C. (Ed.), Applications of Nonlinear and Chaotic Dynamics in Mechanics. Kluwer Academic Publisher, Dordrecht, pp. 373–386.

Stépán, G., 2002. Appell–Gibbs equation for classical wheel shimmy – an energy view. Journal of Computational and Applied Mechanics 3 (1), 85–92.

Stépán, G., Haller, G., 1995. Quasiperiodic oscillations in robot dynamics. Nonlinear Dynamics 8 (4), 513–528.

Szalai, R., Stépán, G., Hogan, S.J., 2006. Continuation of bifurcations in periodic delay-differential equations using characteristic matrices. SIAM Journal on Scientific Computing 28 (4), 1301–1317.

Takács, D., 2005. Dynamics of Rolling of Elastic Wheels. Master's thesis, Department of Applied Mechanics, Budapest University of Technology and Economics, Hungary.

Takács, D., Stépán, G., 2007. Experiments on quasi-periodic wheel shimmy. In: Proceedings of IDETC/CIE 2007, ASME Las Vegas, CD-ROM paper no. DETC2007-35336, pp. 1–8.

Takács, D., Stépán, G., Hogan, S.J., 2008. Isolated large amplitude periodic motions of towed rigid wheels. Nonlinear Dynamics 52 (1–2), 27–34.

Troger, H., Zeman, K., 1984. A nonlinear-analysis of the generic types of loss of stability of the steady-state motion of a tractor-semitrailer. Vehicle System Dynamics 13 (4), 161–172.

Wickert, J.A., Mote Jr., C.D., 1990. Classical vibration analysis of axially moving continua. Journal of Applied Mechanics 57 (3), 738–744.